

Alma Mater Studiorum Università di Bologna
Archivio istituzionale della ricerca

Optimization of sol-immobilized bimetallic Au-Pd/TiO₂ catalysts: reduction of 4-nitrophenol to 4-aminophenol for wastewater remediation

This is the final peer-reviewed author's accepted manuscript (postprint) of the following publication:

Published Version:

Alshammari K., Niu Y., Palmer R.E., Dimitratos N. (2020). Optimization of sol-immobilized bimetallic Au-Pd/TiO₂ catalysts: reduction of 4-nitrophenol to 4-aminophenol for wastewater remediation. PHILOSOPHICAL TRANSACTIONS - ROYAL SOCIETY. MATHEMATICAL, PHYSICAL AND ENGINEERING SCIENCES, 378(2176), 1-14 [10.1098/rsta.2020.0057].

Availability:

This version is available at: <https://hdl.handle.net/11585/765969> since: 2020-07-14

Published:

DOI: <http://doi.org/10.1098/rsta.2020.0057>

Terms of use:

Some rights reserved. The terms and conditions for the reuse of this version of the manuscript are specified in the publishing policy. For all terms of use and more information see the publisher's website.

This item was downloaded from IRIS Università di Bologna (<https://cris.unibo.it/>).
When citing, please refer to the published version.

(Article begins on next page)

This is the final peer-reviewed accepted manuscript of:

Alshammari, K.; Niu, Y.; Palmer, R. E.; Dimitratos, N. Optimization of Sol-Immobilized Bimetallic Au–Pd/TiO₂ Catalysts: Reduction of 4-Nitrophenol to 4-Aminophenol for Wastewater Remediation. Philosophical Transactions of the Royal Society A: Mathematical, Physical and Engineering Sciences 2020, 378 (2176), 20200057.

The final published version is available online at:
<https://doi.org/10.1098/rsta.2020.0057>

Terms of use:

Some rights reserved. The terms and conditions for the reuse of this version of the manuscript are specified in the publishing policy. For all terms of use and more information see the publisher's website.

This item was downloaded from IRIS Università di Bologna (<https://cris.unibo.it/>)

When citing, please refer to the published version.


Optimization of sol-immobilized bimetallic Au–Pd/TiO₂ catalysts: reduction of 4-nitrophenol to 4-aminophenol for wastewater remediation

Khaled Alshammari¹, Yubiao Niu², Richard E. Palmer² and Nikolaos Dimitratos^{1,3}

¹School of Chemistry, Cardiff Catalysis Institute (CCI), Cardiff University, Main Building, Park Place, Cardiff CF10 3AT, UK

²College of Engineering, Swansea University, Bay Campus, Fabian Way, Swansea SA1 8EN, UK

³Dipartimento Chimica Industriale 'Toso Montanari', Università degli Studi di Bologna, Viale Risorgimento 4, 40136, Bologna, Italy

 ND, 0000-0002-6620-4335

A sol-immobilization method is used to synthesize a series of highly active and stable Au_xPd_{1-x}/TiO₂ catalysts (where $x = 0, 0.13, 0.25, 0.5, 0.75, 0.87$ and 1) for wastewater remediation. The catalytic performance of the materials was evaluated for the catalytic reduction of 4-nitrophenol, a model wastewater contaminant, using NaBH₄ as the reducing agent under mild reaction conditions. Reaction parameters such as substrate/metal and substrate/reducing agent molar ratios, reaction temperature and stirring rate were investigated. Structure-activity correlations were studied using a number of complementary techniques including X-ray powder diffraction, X-ray photoelectron spectroscopy and transmission electron microscopy. The sol-immobilization route provides very small Au–Pd alloyed nanoparticles, with the highest catalytic performance shown by the Au_{0.5}Pd_{0.5}/TiO₂ catalyst.

This article is part of a discussion meeting issue 'Science to enable the circular economy'.

1. Introduction

The reduction of 4-nitrophenol (4-NP) to 4-aminophenol (4-AP) is a model reaction for evaluating the catalytic activity of nanomaterials. Moreover, 4-NP is considered one of the most toxic water pollutants; therefore, the successful transformation to another chemical product is highly interesting for both industry and academia [1–5]. 4-NP is derived from many processes in the industry, such as agro chemistry, pigments and pharmaceutical factories [6–9]. Owing to its high toxicity, new methods to remove this compound from the environment are desirable, such as the direct conversion of 4-NP with reductant in the presence of metal nanoparticles (NPs) to produce 4-AP [10].

The 4-AP molecule is less toxic and is a useful chemical in many industrial applications, such as in drugs (analgesic and antipyretics) and corrosion inhibitors [8,11]. Owing to the simplicity of the reduction of 4-NP using sodium borohydride (NaBH_4) as a reducing agent in excess, it has become a model reaction for catalytic studies. The reaction can be easily monitored using UV–Vis spectroscopy by observing the decrease in the absorption of the 4-nitrophenolate anion at 400 nm [12]. The conversion and rate constant of the reaction can be calculated. In addition, there is only one product (4-AP) for this reaction and no by-products are formed [13,14]. Furthermore, it can be catalysed by any immobilized or indeed free NPs in aqueous solution under mild reaction conditions [12,15]. Although this reaction is thermodynamically favourable at ambient conditions, it is kinetically hindered without catalyst, since the reduction potential of 4-NP to 4-AP is $E^\circ = 0.76 \text{ V}$, while that of borate to borohydride ($\text{H}_3\text{BO}_3/\text{BH}_4^-$) is $E^\circ = -1.33 \text{ V}$ [13,16].

Gold NPs, free or immobilized onto the desired support, have been investigated under mild conditions for the reduction of 4-NP [1–5]. Generally, the catalytic activity of gold NPs depends significantly on several factors including particle size [17,18], metal loading [19] and shape of the NPs used. It has been shown that when alloying gold with another metal, such as palladium or platinum, the catalytic activity significantly improves, due to a synergistic effect between the two metals [15]. Thus, Au NPs are often combined with other metals to prepare bimetallic catalysts of high catalytic performance, traceable to changes in the interface electronic structure [20]. Examples of such bimetallic systems with excellent catalytic activity, reusability and stability are Ag–Au core–shell NPs, Ag–Au NP alloys and alloy–graphene hybrids [21–23].

Despite the excellent catalytic activities reported for the above-mentioned bimetallic systems, Pd based NPs have undoubtedly exhibited the best overall catalytic performance for the hydrogenation of 4-NP [24]. Previous studies showed that Pd-based bimetallic NPs are more effective than Pt–Au bimetallic NPs [25–29]. Alloying of Au–Pd results in modifying electronic and surface properties and in turn the adsorption and activation for substrates and thus yielding relatively faster reaction rate constants compared to Au–Pt alloys [25]. However, very limited studies are reported for the reduction of 4-NP over Au–Pd bimetallic systems [30–32].

Chen *et al.* [33] studied the catalytic activity of atomic ratios of Au and Pd in bimetallic NPs for the reduction of 4-NP by synthesizing Au–Pd NPs supported on graphene nanosheets (GNs). They reported that the activity of bimetallic Au–Pd/GN catalyst was higher than monometallic Au/GN and Pd/GN catalysts by factors of 8 and 5, respectively, attributed to a synergistic effect between Au and Pd species. Moreover, Au–Pd with molar ratio (1 : 1) showed the highest activity. A similar Au–Pd ratio was reported for the same reaction by Fang *et al.* [31], who synthesized Au–Pd bimetallic NPs deposited on ultrathin graphitic carbon nitride nanosheets. However, recent work by Srisombat *et al.* [34] has shown a different optimal atomic ratio for Au–Pd bimetallic catalysts, where the highest catalytic activity was obtained with Au:Pd atomic ratio 1 : 4 [35]. They concluded that the catalytic activity strongly depends not only on chemical constituents of the catalyst, but also on the size of the Au–Pd NPs.

The sol-immobilization method using PVA and NaBH_4 as stabilizing and reducing agents, respectively, is an effective method to prepare small metal NPs with a narrow particle size distribution, compared with conventional techniques such as wet impregnation and deposition–precipitation. Rogers *et al.* [12] prepared monometallic 1 wt% Pd/ TiO_2 by the sol-immobilization method using PVA stabilizer and NaBH_4 reductant for the hydrogenation of 4-NP to 4-AP and

reported high activity compared with other catalysts prepared by different methods. For example, the turnover frequency (TOF) for 1%Pd/TiO₂ in their work was 247 h⁻¹, while Sun *et al.* [36] reported TOF of 70 h⁻¹ for a 5 wt% Pd/C.

This work is focused on optimizing the reaction parameters affecting the aqueous phase hydrogenation of 4-NP using a range of supported gold–palladium NPs on TiO₂ (P25), where the Au–Pd atomic ratio is also varied. The catalysts have been prepared using the sol-immobilization method, and reaction parameters were optimized using a series of catalysts with different Au and Pd atomic ratio using sodium borohydride as a reducing agent under mild reaction conditions. Experimental parameters, such as concentration of 4-NP, NaBH₄ and catalyst, stirring rate and Au/Pd molar ratio) have been studied and optimized to achieve the best catalyst performance. The most active catalyst was also tested for the hydrogenation of 4-NP using different reducing agents (hydrogen donors), such as hydrous hydrazine and formic acid. The promising catalytic results obtained showed the high potential of using alternative ‘green’ hydrogen donors for the effective hydrogenation of 4-NP to 4-AP.

2. Methods

(a) Materials

K₂PdCl₄ (Sigma-Aldrich, 99%), HAuCl₄·3H₂O (Alfa Aesar, 99.99%), 4-NP, O₂NC₆H₄OH (Sigma-Aldrich, 99.99%), Polyvinyl alcohol (PVA, MW = 10 000, Sigma-Aldrich, 99%), sulfuric acid, H₂SO₄ (Fisher, 95%), NaOH (Fisher, 99%) and TiO₂ (P25, Degussa greater than 99.5%). All chemicals were used as received.

(b) Catalyst preparation

A series of Au_xPd_{1-x}/TiO₂ catalysts (where $x=0, 0.25, 0.5, 0.75, 0.87$ and 1) were prepared using the sol-immobilization method [13]. The total nominal metal weight loadings were kept constant at a value of 1 wt% for all catalysts. As an example, to prepare 1 wt% of Au_{0.5}Pd_{0.5}/TiO₂ catalyst, an aqueous solution of K₂PdCl₄ (0.64 ml of 5.5 mg ml⁻¹ stock) and HAuCl₄·3H₂O (0.53 ml of 12.25 mg ml⁻¹ stock) were placed into a beaker containing 400 ml of deionized water under vigorous stirring. Subsequently, a required amount of polyvinyl alcohol (PVA, 1 wt% in 10 ml of fresh stock) was added to maintain PVA/total metal (w/w) = 0.65. Solution of NaBH₄ (0.1 M; NaBH₄/total metal (mol mol⁻¹) = 5) was freshly prepared in deionized water and added dropwise to the reaction mixture over a 1 min period with stirring to form dark brown-black sols. After completing the co-reduction of Au and Pd species (30 min of stirring), the colloidal solution was immobilized on TiO₂ (commercial P25) under vigorous stirring conditions. The required amount of TiO₂ support was calculated to give a final total metal loading of 1 wt%. The mixture was acidified to pH 1–2 by sulfuric acid before being stirred for 1 h to accomplish full immobilization of the metal NPs (table 1).

(c) Characterization

X-ray diffraction (XRD) patterns were recorded using a PANalytical X-PertPro X-ray diffractometer. A Cu K_{α1} X-ray radiation source run at 40 kV and 40 mA fitted with an X'Celerator detector was used. The diffraction patterns were recorded from 5 to 80° of 2θ with a step size of 0.017°. X-ray photoelectron spectroscopy (XPS) was carried out using a Kratos Axis Ultra DLD XPS system equipped with a monochromatic Al K_α X-ray source operating at 300 W. Data were collected with pass energies of 160 eV for survey spectra and of 40 eV for the high-resolution scans. Samples were mounted using double-sided adhesive tape and binding energies were calibrated to C1s binding energy of carbon taken as 284.7 eV. Peaks were fitted as Gaussian Lorentzian curves GL(30) using CasaXPS software. Scanning electron microscopy (SEM) images were captured using Hitachi TM3030PLUS equipped with a Quantax70 energy-dispersive X-ray

Table 1. List of prepared catalysts and total metal loadings (wt%) and Au/Pd (mol mol⁻¹) extracted from MP-AES and EDS analyses.

catalysts	metal loadings (wt%)		Au/Pd (mol mol ⁻¹)		<i>S</i> _{BET} (m ² g ⁻¹)
	MP-AES	EDS	MP-AES	EDS	
Au/TiO ₂	0.99	0.96	100:0	100:0	58 (±3)
Au _{0.13} Pd _{0.87} /TiO ₂	0.96	0.98	11:89	9:91	57 (±4)
Au _{0.25} Pd _{0.75} /TiO ₂	0.97	0.99	27:73	20:80	
Au _{0.5} Pd _{0.5} /TiO ₂	0.95	0.98	51:49	52:48	
Au _{0.75} Pd _{0.25} /TiO ₂	0.98	0.98	76:24	74:26	
Au _{0.87} Pd _{0.13} /TiO ₂	0.97	0.97	84:16	86:14	
Pd/TiO ₂	0.94	0.98	0:100	0:100	55 (±1)

spectroscopy (EDS). The powder samples were placed on the carbon tape which was attached to the sample holder. Transmission electron microscopy (TEM) images were taken using a FEI F200x (Talos) TEM operating at 200 kV. Samples were prepared by dispersing the catalyst powder in high purity ethanol using ultra-sonication then 50 µl of the suspension was dropped onto a holey carbon film supported by a 300-mesh copper TEM grid followed by the evaporation of the solvent. Mean particle size and particle size distribution was calculated by counting 300 particles using the ImageJ software. UV–Vis spectra were recorded in 1 cm² quartz cuvette using *in situ* AvaSoft UV–Vis spectrometry and a Q-blue wireless temperature controller (Ava-light-DH-S-BAL combined deuterium–halogen as light sources and Avantes ULS2048-USB2-UA-50 as a detector). All measurements were recorded in the range of 200–800 nm at room temperature. For each series of measurements, the absorption of distilled water is measured as the reference baseline and subtracted from each measurement. All the obtained UV–Vis spectra were manually normalized at 600 nm to zero.

(d) Evaluation of catalytic performance

(i) Calibration

The molar extinction coefficient was estimated by preparing a fresh solution of 4-NP with a concentration of 9.3×10^{-3} M, which was subsequently diluted to make solutions with final concentrations between 1.256×10^{-4} M and 5×10^{-6} M. A 0.05 M aqueous solution of NaBH₄ was freshly prepared by adding 0.0474 g NaBH₄ into a 25 ml volumetric flask. A 0.3 ml bolus of this solution was added to the 1 cm² cuvette. A fresh solution of NaBH₄ was prepared prior to each reaction due to its rapid decomposition. The calibration curve was plotted and the molar extinction coefficient of 18 620 (M⁻¹ cm⁻¹) was given, which is close to the reported value, 18 000 (M⁻¹ cm⁻¹) [24,33].

(ii) Kinetic studies

The catalytic performance of the synthesized catalysts was evaluated in the reduction of 4-NP by NaBH₄ as a model reaction. The reaction was carried out in aqueous phase under mild conditions (*T* = 30°C, atmospheric pressure and stirring rate of 1000 r.p.m). To maintain a pseudo-first order reaction kinetics, a large excess of NaBH₄ over 4-NP was used (optimized molar ratio of NaBH₄/4-NP = 30). In a typical, *in situ*, testing, 0.3 ml of NaBH₄ (3.6×10^{-2} M) was transferred into 1 cm² quartz corvette containing the catalyst and solution of 4-NP (2.7 ml, 1.35×10^{-4} M, 4-NP/metal molar ratio = 13). The total volume of the reaction mixture was 3 ml. At different time interval, UV–Vis measurements were taken in the range of 200–800 nm using AvaSoft

UV–Vis spectrometry and the absorbance at 400 nm was recorded and then used as an indication of the decay in 4-NP concentration as a function of reaction time (up to 30 min). Apparent rate constants (K_{app} , min^{-1}) were calculated for each catalyst under investigation and used for the activity comparisons.

3. Results and discussions

(a) X-ray diffraction

Figure 1 shows the XRD patterns for Au/TiO₂, Pd/TiO₂ and Au_xPd_{1-x}/TiO₂ catalysts as well as for bare TiO₂ support. All diffraction patterns match well with the diffraction pattern for commercial TiO₂ (P25), which is a mixture of anatase (80–85%) and rutile (20–15%) phases. The diffraction peaks at 27.5°, 36.2°, 54.5° and 69.2° correspond to the presence of the rutile phase (JCPDS No. 21-1276) [37], whereas diffraction peaks at $2\theta = 25.3^\circ$, 48.0°, 53.8° and 62.6° correspond to the presence of the anatase phase (JCPDS No. 21-1272) [37]. No evidence for any other phases upon the inclusion of Au and/or Pd NPs are presented. The diffraction peaks for any metallic Au phases would be expected at $2\theta = 38.2^\circ$, 44.4°, 64.6° and 77.5° for (111), (200), (220) and (311) planes, respectively (JCPDS No. 04-0784) [38]. Also, diffraction peaks of any metallic Pd phases would be expected to be at $2\theta = 40.4^\circ$, 46.9° and 68.6°, which correspond to the Pd (111), (200) and (220) phases, respectively, (JCPDS No. 01-087-0645) [38]. The absence of any diffraction peaks for metallic Au and/or Pd phases suggests the confinement of these NPs in small crystallite sizes which is below the detection limit of XRD instrument (less than 5 nm). These findings are expected for the sol-immobilization route used for preparing very small supported NPs [12,39], which will be confirmed later by TEM results. Moreover, the high metal dispersion on the TiO₂ support could also contribute to this observation, which is consistent with the data obtained by SEM-EDS (see electronic supplementary material, figure S3).

(b) TEM analysis

TEM images presented in figure 2 show the distribution of Au and Pd NPs immobilized on TiO₂ exhibiting relatively good dispersion and narrow particle size range. No obvious sign of serious aggregation could be seen over any catalysts. Moreover, the shape of the particles is almost spherical to hemispherical for all catalysts. The inset graphs in figure 2 show the particle size distributions in the range of 1–6 nm, for monometallic Au/TiO₂ and Pd/TiO₂ catalysts. The mean particle size in diameter of the supported bimetallic Au_xPd_{1-x} NP samples are between 2.07 (± 0.61 s.d.) and 3.20 (± 1.10 s.d.) nm according to their projected surface areas. However, Au_{0.5}Pd_{0.5}/TiO₂ catalyst presents the narrowest particle size range (1–4 nm) and the smallest mean particle size (approx. 2 nm in diameter) with a uniform spherical shape compared with other Au and Pd combinations. These results are in good agreement with a recent study by Cattaneo *et al.* [39], who synthesized Au_{0.5}Pd_{0.5}/TiO₂ with small mean particle size (2.1 nm) by using the sol-immobilization method. The mean particle size of all catalysts is summarized in table 2. As we can observe from table 2, atomic ratio of Au : Pd = 1 : 1 is the optimum for obtaining small mean metal particle size.

(c) X-ray photoelectron spectroscopy analysis

XPS analysis is employed to look further insight metal speciation, oxidation states and surface compositions of supported Au_xPd_{1-x} NPs. The XPS profile of TiO₂ support (electronic supplementary material, figure S4) is also presented and results show that deposition of metal NPs did not alter Ti⁴⁺ oxidation state of the support, which are in agreement with previous reported data [40]. XPS core level spectra of Au(4f) and Pd(3d) are presented in figure 3a and figure 3b, respectively. Their corresponding refined data are summarized in table 2. Figure 3a shows the XPS core level spectra of all catalysts at Au(4f) region, which can be identified by the

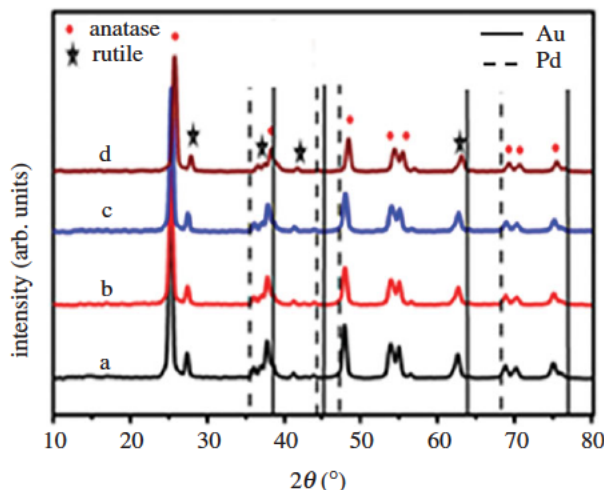


Figure 1. XRD patterns for (a) bare TiO_2 , (b) Au/TiO_2 , (c) Pd/TiO_2 and (d) $\text{Au}_{0.5}\text{Pd}_{0.5}/\text{TiO}_2$ materials. No diffractions were found for Au (solid lines) or Pd (dashed lines) over all materials. (Online version in colour.)

two peaks of $\text{Au } 4f_{7/2}$ and $\text{Au } 4f_{5/2}$ [41]. The binding energy (BE) of $\text{Au } 4f_{7/2}$ peak is located in the range of 83.5–83.1 eV and thus suggesting the presence of Au in a metallic state over all catalysts [39,42]. This is expected for the sol-immobilization route being used for the preparation [43,44] due to the role of capping agent (PVA) for protecting and stabilizing the formed metal NPs.

The BE of $\text{Au } 4f_{7/2}$ (83.5 eV), monometallic Au/TiO_2 catalyst, is lower than that of bulk gold metal (84.0 eV) [39]. This slight decrease in binding energy can be attributed to particle size effects and presence of negative charged gold NPs ($\text{Au}^{\delta-}$) [45–47]. A decrease of BE in the range of –0.2 to –1.2 eV, is mainly attributed due to the formation of Au NPs with NPs size below 3 nm [48]. In addition, the electron transfer from support to Au particles and hence strong metal-support interaction (SMSI) can be a reason for the observed reduction in BE at $\text{Au } 4f_{7/2}$ peak [49]. The XPS core level spectra at $\text{Au}(4f)$ region suggest the formation of very small and/or alloyed NPs.

Upon the inclusion of Pd atoms and thus formation of $\text{Au}_x\text{Pd}_{1-x}/\text{TiO}_2$ catalysts, more shift in BE was observed. As it can be seen in table 2, $\text{Au}_{0.87}\text{Pd}_{0.13}/\text{TiO}_2$ catalyst with the lowest Pd contents exhibited a shift of 0.63 eV in BE compared to bulk Au (4f) spectra. The most pronounced shift was approximately 0.9 eV with the highest Pd contents catalyst ($\text{Au}_{0.13}\text{Pd}_{0.87}/\text{TiO}_2$). These results suggest the formation of very small sizes of alloyed NPs and thus strong interaction between Au and Pd atoms [38,39,50].

To better understanding the structure–activity correlations at the surface of catalysts, XPS core level spectra at $\text{Pd}(3d)$ region were also measured over all catalysts (figure 3b). Refined data are also presented in table 2. Two peaks can be assigned for $\text{Pd}(3d)$ region: $\text{Pd } 3d_{5/2}$, and $\text{Pd } 3d_{3/2}$ [51]. Palladium in metallic state (Pd^0) is the predominant component for all bimetallic combinations, while a mixture of metallic (Pd^0 at 334.99 eV) and oxidic (Pd^{II} at 337 eV) with ratio ($\text{Pd}^{\text{II}}/\text{Pd}^0$) of 20% are found in monometallic Pd/TiO_2 catalyst (figure 3 and table 2). Similar findings were reported by Rogers *et al.* [12] for Pd/TiO_2 prepared by sol-immobilization method figure 4.

(d) Catalytic activity of $\text{Au}_x\text{Pd}_{1-x}/\text{TiO}_2$ catalysts

It was reported that the addition of Pd to Au enhances the activity and selectivity in several reactions [33,39]. In general, bimetallic catalysts are found to be more active than their monometallic counterparts; therefore, there is growing interest in studying and understanding this subject [15,39]. The enhanced activity can be related to many factors including the electronic and geometric effects. The former increases the binding of adsorbates to metal surfaces, while

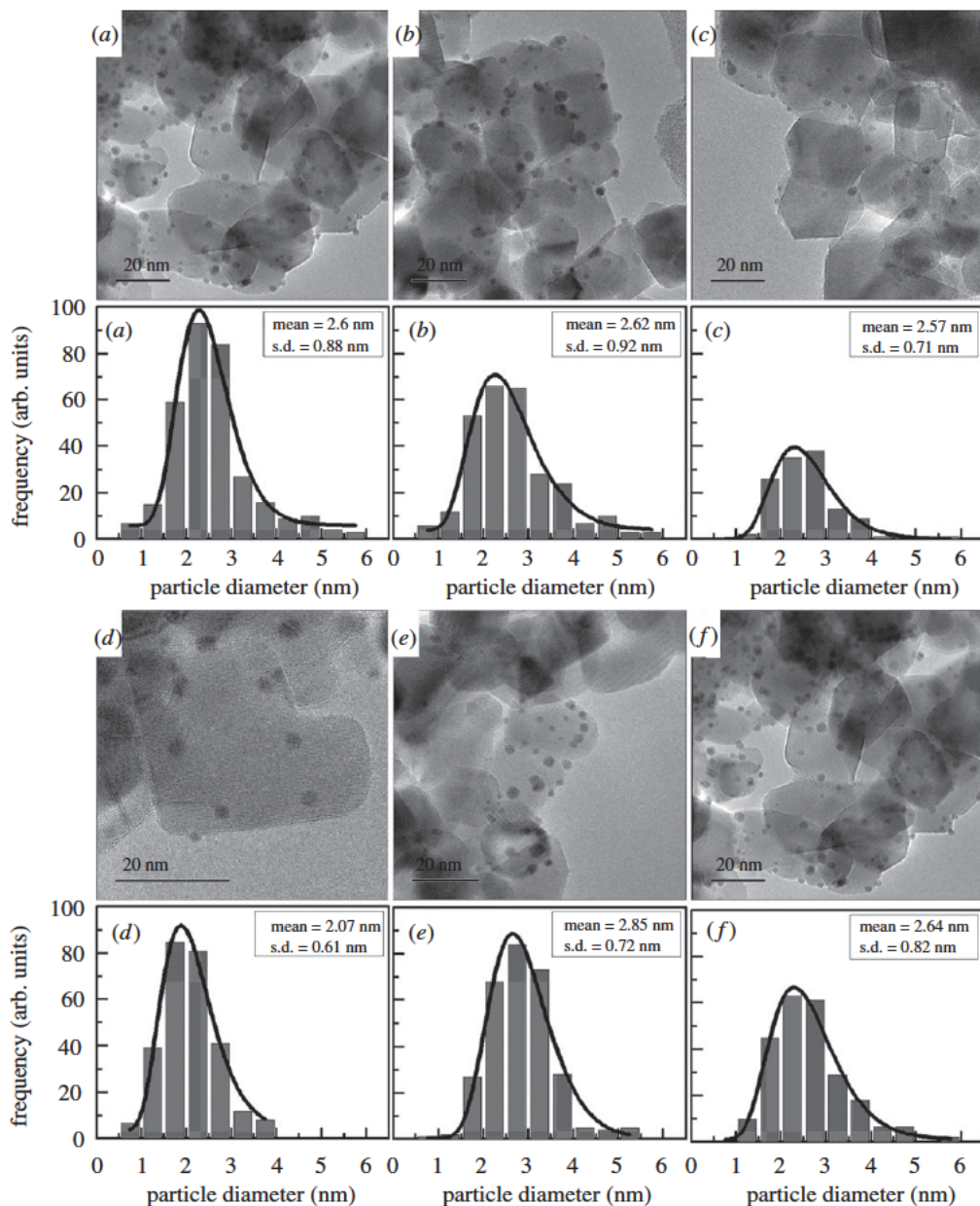


Figure 2. TEM images and metal particle size distributions (inset) obtained for (a) Au/TiO₂, (b) Pd/TiO₂, (c) Au_{0.87}Pd_{0.13}/TiO₂, (d) Au_{0.5}Pd_{0.5}/TiO₂, (e) Au_{0.25}Pd_{0.75}/TiO₂ and (f) Au_{0.13}Pd_{0.87}/TiO₂ catalysts.

the later belongs to restructuring and rearrangements of active components on the support. Therefore, we believe that the bimetallic combinations of Au and Pd on the surface of support influence reaction rates and kinetic pathways of a given reaction. So far, sol-immobilization method was used to prepare a series of Au_xPd_{1-x}/TiO₂ catalysts (where $x=0, 0.13, 0.25, 0.5, 0.75, 0.87$ and 1) for the reduction of 4-NP by NaBH₄.

The reduction of 4-NP by NaBH₄ was chosen as a model reaction to examine the catalytic activity and performance optimization of Au_xPd_{1-x}/TiO₂ catalysts (where $x=0, 0.13, 0.25, 0.5, 0.75, 0.8$ and 1). However, and before starting the screening tests, the reaction parameters, such as (i) 4-NP/metal molar ratio, (ii) /NaBH₄/4-NP molar ratio, (iii) NaOH concentration, and (iv)

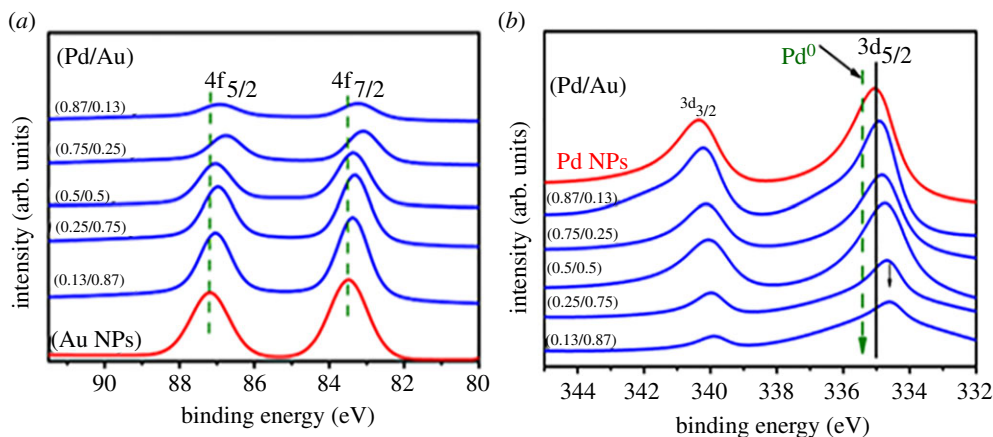


Figure 3. XPS core level spectra at (a) Au(4f) and (b) Pd(3d) regions obtained for monometallic Au/TiO₂ and Pd/TiO₂, catalysts together with different bimetallic Au_xPd_{1-x}/TiO₂ catalysts. (Online version in colour.)

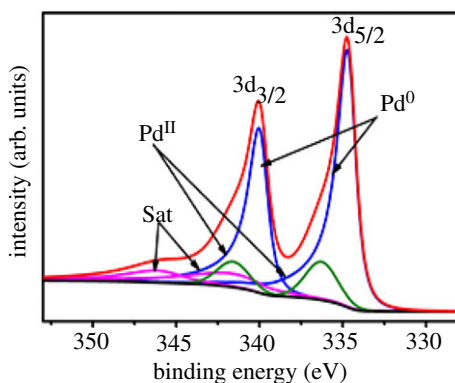


Figure 4. Representative example for XPS core level spectra fitting of Pd(3d) for Pd/TiO₂ catalyst. (Online version in colour.)

Table 2. BE (eV) and their shifts (in parentheses) for Au 4f_{7/2} and Pd 3d_{5/2} regions obtained for mono- and bimetallic Au and Pd catalysts. Mean particle sizes (nm) with standard deviation (in parentheses) extracted from TEM analysis are also presented.

catalyst	BE in eV (chemical shifts)		mean size in nm (s.d.)	Pd ^{III} /Pd ⁰ Fractions
	Au4f _{7/2}	Pd3d _{5/2}		
Au/TiO ₂	83.5 (0.5)	—	2.60 (0.88)	—
Au _{0.87} Pd _{0.13} /TiO ₂	83.37 (0.63)	334.56 (0.84)	2.57 (0.71)	0
Au _{0.75} Pd _{0.25} /TiO ₂	83.35 (0.65)	334.64 (0.76)	3.20 (1.10)	0
Au _{0.5} Pd _{0.5} /TiO ₂	83.31 (0.69)	334.69 (0.71)	2.07 (0.61)	0
Au _{0.25} Pd _{0.75} /TiO ₂	83.22 (0.78)	334.77 (0.63)	2.85 (0.72)	0
Au _{0.13} Pd _{0.87} /TiO ₂	83.1 (0.9)	334.89 (0.51)	2.64 (0.82)	0
Pd/TiO ₂	—	334.99 (0.41)	2.62 (0.92)	0.2

stirring rate, were first optimized over monometallic 1 wt% Au/TiO₂ catalyst (see electronic supplementary material for more details). Accordingly, the following reaction conditions were chosen after optimization and used throughout this work for evaluating the activity of the

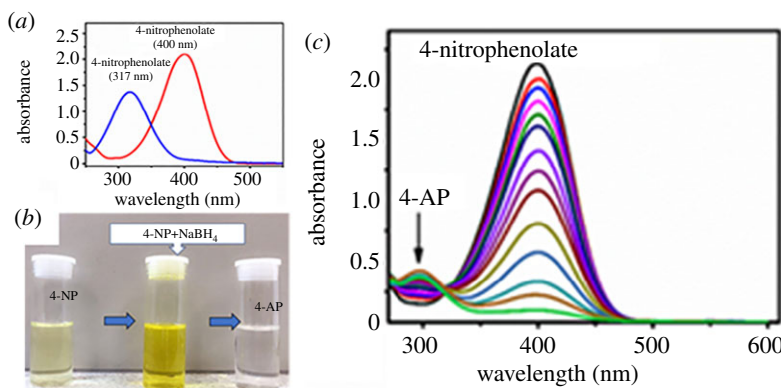


Figure 5. Typical activity testing: (a) UV–Vis spectrum with no catalyst before and after addition of NaBH₄, (b) 4-NP colour changes before and after reduction and (c) UV–Vis spectra during the reduction of 4-NP by NaBH₄ and formation of 4-AP over 1 wt% Au/TiO₂ catalyst. (Online version in colour.)

synthesized catalysts; 4-NP/metal molar ratio = 13, NaBH₄/4-NP molar ratio = 30, $T = 30^{\circ}\text{C}$ and stirring rate = 1000 r.p.m.

Figure 5 shows a typical activity measurement over 1 wt% Au/TiO₂ catalyst. Blank 4-NP solution showed absorption band at approximately 317 nm. After the addition of fresh solution of NaBH₄, the absorption peak was shifted to 400 nm (figure 5a) due to the formation of nitrophenolate anion accompanied by a colour change from light to dark yellow (figure 5b). This peak was remained unaltered over time (examined for approx. 24 h), which suggests that the reaction does not proceed without a catalyst [52–54]. Subsequently, the reduction of 4-NP by NaBH₄ over the prepared catalysts (1 wt% Au/TiO₂ as an example) was then monitored by measuring the changes in the absorbance at 400 nm as a function of time and emerging of a new peak at approximately 300 nm for the product formation, 4-AP (figure 5c).

(i) Kinetic studies

In these experiments, the concentration of NaBH₄ is significant much higher than that of 4-NP (4-NP/NaBH₄ = 30) so it could be considered that the reaction rate could be nearly independent of the NaBH₄ concentration. Thus, a pseudo-first order reaction kinetics could be applied to evaluate the apparent rate constant (K_{app}) for the hydrogenation of 4-NP [31,55]. For the reduction of 4-NP, the ratio of its concentration at time = t (C_t) to the initial value at $t = 0$ (C_0) could be directly calculated by the ratio of their corresponding absorbance: A_t/A_0 (where A = absorbance at 400 nm). So far the kinetic equation for the reduction of 4-NP could then be written as

$$\frac{dC_t}{dt} = -K_{\text{app}}C_t \quad \text{or} \quad \ln\left(\frac{C_t}{C_0}\right) = \ln\left(\frac{A_t}{A_0}\right) = -K_{\text{app}}t.$$

The plot between $\ln(A_t/A_0)$ as y -axis and time as x -axis can provide us the value of K_{app} , as shown in figure 6a over 1 wt% Au/TiO₂ catalyst as a representative example.

The catalytic performance of all catalysts was evaluated for the reduction of 4-NP by NaBH₄ under the same optimized mild reaction conditions and the corresponding K_{app} values were obtained and used for activity comparisons in agreement with the experimental procedure reported in literature [12]. For simplicity, the K_{app} values (in min^{-1}) were plotted as a function of Pd mole fractions. As a result, a volcano like-shape curve is obtained, as shown in figure 6b.

As can be seen, the activity increased significantly from 0.14 (for Au/TiO₂) to 0.22 min^{-1} when the Pd content was increased from 0 to 0.13 (Au_{0.87}Pd_{0.13}/TiO₂ catalyst). Further increase of Pd content was accompanied with a significant increase in the K_{app} until reached a maximum value of 0.38 min^{-1} with Au:Pd atomic ratio of 1 : 1 (Au_{0.5}Pd_{0.5}/TiO₂ catalyst). Further increase of Pd

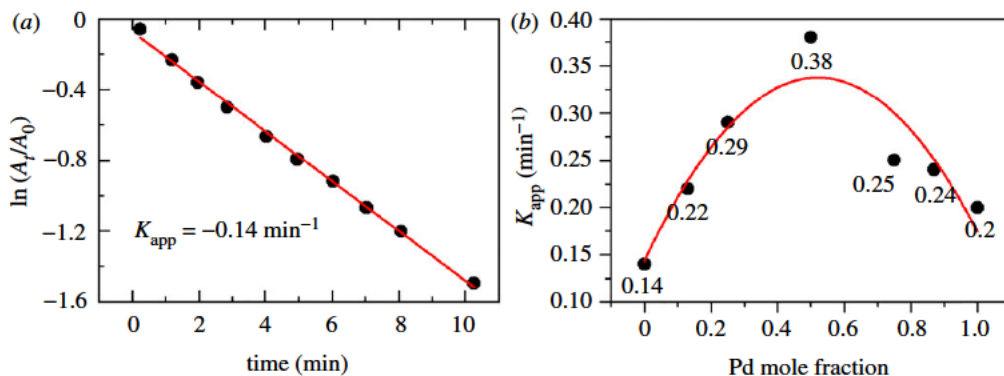


Figure 6. (a) $\ln(A_t/A_0)$ as a function of time (minutes) for the reduction of 4-NP by NaBH_4 over 1 wt% Au/TiO_2 , as a representative example, (b) K_{app} (min^{-1}) as a function of Pd mole fraction over different $\text{Au}_x\text{Pd}_{1-x}/\text{TiO}_2$ catalysts. Reaction condition: 4-NP/metal molar ratio = 13, NaBH_4 /4-NP molar ratio = 30, $T = 30^\circ\text{C}$ and stirring rate = 1000 r.p.m. (Online version in colour.)

content led to a progressive decrease of the K_{app} from 0.38 to 0.2 min^{-1} . It is evident that a volcano type catalytic behaviour with supported Au–Pd NPs for the catalytic reduction of 4-NP to 4-AP using NaBH_4 as the reducing agent.

The enhanced catalytic activity of $\text{Au}_{0.5}\text{Pd}_{0.5}/\text{TiO}_2$ catalyst can be linked to several factors such as Au–Pd NPs size, synergistic effect and/or it could be related to the structure of alloyed NPs that can be formed at this specific composition as it has been shown in previous reported studies [56]. According to the TEM results, Au–Pd NPs prepared with molar ratio of 1:1 produced, the smallest particles (approx. 2 nm) with the narrowest particle size distribution from 2 to 4 nm compared with other metal molar ratios. However, statistically, the difference in particle size between bimetallic catalysts is not that significant to allow us to draw a conclusion (the mean particle size was between $2.07 (\pm 0.61)$ and $3.20 (\pm 1.10)$ nm). Another factor that can help us to understand the structure–activity correlations is the electron transfer between bimetallic Au–Pd systems at different molar ratio. XPS data showed that the level of interaction between both metals increases with increasing Pd molar ratio to a certain degree, since the binding energy of Au and Pd decrease. However, it was not able to explain the low activity of $\text{Au}_{0.13}\text{Pd}_{0.87}/\text{TiO}_2$, which has the highest Pd molar ratio of all catalysts.

To further investigating the structure–activity correlations of Au–Pd NPs, a characterization by high-angle annular dark-field scanning transmission electron microscopy (HAADF-STEM) and EDS mappings were conducted on the surface of $\text{Au}_{0.13}\text{Pd}_{0.87}/\text{TiO}_2$, $\text{Au}_{0.5}\text{Pd}_{0.5}/\text{TiO}_2$ and $\text{Au}_{0.87}\text{Pd}_{0.13}/\text{TiO}_2$ catalysts (see electronic supplementary material, figure S8). The results clearly show the presence of random Au–Pd alloyed NPs on the surface along with the presence of single Au and Pd NPs of all bimetallic catalysts with the highest alloy population (52%) observed for $\text{Au}_{0.5}\text{Pd}_{0.5}/\text{TiO}_2$ catalysts. In the case of $\text{Au}_{0.13}\text{Pd}_{0.87}/\text{TiO}_2$ and $\text{Au}_{0.87}\text{Pd}_{0.13}/\text{TiO}_2$ catalysts, the population of Au–Pd alloyed NPs was 25% and 10%, respectively. Thus, the higher population of Au–Pd alloyed NPs could be considered as an explanation of such highest activity observed for $\text{Au}_{0.5}\text{Pd}_{0.5}/\text{TiO}_2$ catalyst in respect to the other stoichiometric atomic ratios.

Reusability tests were conducted on the most active catalyst ($\text{Au}_{0.5}\text{Pd}_{0.5}/\text{TiO}_2$). As shown in electronic supplementary material, figure S9, a good stability was maintained and conversion (%) over four cycles was dropped only from 80 to 75%. No leaching was detected for Au and Pd NPs in the reaction medium using MP-AES. TEM images on used $\text{Au}_{0.5}\text{Pd}_{0.5}/\text{TiO}_2$ catalyst (electronic supplementary material, figure S10) showed good dispersion of supported Au–Pd NPs throughout the four cycles without any significant agglomeration. However, very tiny changes in the mean particle size could be noted (2.07 ± 0.61 to 2.2 ± 0.73 nm). Nevertheless, the average diameter of Au–Pd NPs is still very small without showing significant agglomeration.

Furthermore, XPS analysis on the used catalyst revealed that the surface atomic ratio of both Au and Pd NPs are in metallic state (Au:Pd = 53:47) with no significant changes when compared to the fresh catalysts (Au:Pd = 46:54). This suggests the high stability of the prepared NPs using the sol-immobilization route.

4. Conclusion

The sol-immobilization method was successfully used to immobilize a series of 1 wt% of $\text{Au}_x\text{Pd}_{1-x}$ NPs (where $x = 0, 0.13, 0.25, 0.5, 0.75, 0.87$ and 1) onto TiO_2 , (P25-commercial support), as the chosen support. The catalytic performance of the prepared supported NPs in the catalytic reduction of 4-NP to 4-AP under mild reaction conditions was evaluated focusing on the structural optimization of Au–Pd supported bimetallic NPs by varying Au:Pd atomic ratio. The catalytic results showed that monometallic Pd NPs are more active than Au under the same reaction conditions ($K_{\text{app}} = 0.2$ and 0.14 min^{-1} for monometallic Pd and Au, respectively). However, the inclusion of Pd atoms into Au NPs and thus formation of Au–Pd alloy NPs significantly enhanced the catalytic performance compared with the monometallic Au and Pd catalysts, with the highest activity observed for the synthesized $\text{Au}_{0.5}\text{Pd}_{0.5}/\text{TiO}_2$ catalyst ($K_{\text{app}} = 0.38 \text{ min}^{-1}$). TEM and STEM results clearly showed the formation of random alloy Au–Pd NPs in all the bimetallic catalysts, with the smallest narrowest size ranges observed for $\text{Au}_{0.5}\text{Pd}_{0.5}/\text{TiO}_2$ catalyst, which might be responsible for the highest activity. These results suggest that incorporation of small additives of Au atoms to Pd atoms can significantly enhance the catalytic activity and stability when compared with the monometallic counterparts, in the case of the hydrogenation of 4-NP to 4-AP.

Data accessibility. The datasets supporting this article have been uploaded as part of the electronic supplementary material.

Authors' contributions. K.A. synthesized the catalysts and carried out catalytic evaluation. K.A. carried out XPS, XRD, SEM, UV–Vis, TEM analysis and helped with the interpretation. Y.N. carried out TEM analysis and helped with the interpretation. N.D. supervised and designed the experiments and was involved in the writing and editing of the manuscript. K.A., Y.N. and R.P. were involved in the writing and editing of the manuscript.

Competing interests. The authors declare no conflict of interest.

Acknowledgements. The authors would like to thank Cardiff University, UK, for use of facilities and support by their staff. The authors would also acknowledge the Advanced Imaging of Materials (AIM) facility at Swansea University, UK, for the support The Forensic Medicine Centres and Ministry of Interior in Riyadh, Saudi Arabia, are acknowledged for their financial support. Special thanks must go to the Saudi Arabian Cultural Bureau office and their staff for the help and support.

References

1. Shen W, Qu Y, Pei X, Li S, You S, Wang J, Zhang Z, Zhou J. 2017 Catalytic reduction of 4-nitrophenol using gold nanoparticles biosynthesized by cell-free extracts of *Aspergillus* sp. WL-Au. *J. Hazard. Mater.* **321**, 299–306. (doi:10.1016/j.jhazmat.2016.07.051)
2. Farrag M, Ibrahim S. 2017 Size selected gold cluster supported alumina as catalyst in reduction of 4-nitrophenol to 4-aminophenol. *J. Nanotechnol. Adv. Mater. Int. J.* **5**, 57–65. (doi:10.18576/jnam/050203)
3. Zhao X, Li Z, Deng Y, Zhao Z, Li X, Xia Y. 2017 Facile synthesis of gold nanoparticles with alginate and its catalytic activity for reduction of 4-nitrophenol and H_2O_2 detection. *Materials (Basel)* **10**, 557. (doi:10.3390/ma10050557)
4. Ansar SM, Kitchens CL. 2016 Impact of gold nanoparticle stabilizing ligands on the colloidal catalytic reduction of 4-nitrophenol. *ACS Catal.* **6**, 5553–5560. (doi:10.1021/acscatal.6b00635)
5. Ma T, Yang WS, Liu SM, Zhang HJ, Liang F. 2017 A comparison reduction of 4-nitrophenol by gold nanospheres and gold nanostars. *Catalysts* **7**, 38–47. (doi:10.3390/catal7020038)
6. Prati L, Martra G. 1999 New gold catalysts for liquid phase oxidation. *Gold Bull.* **32**, 96–101. (doi:10.1007/bf03216617)

7. Zhang B, Yuan Y, Philippot K, Yan N. 2015 Ag–Pd and CuO–Pd nanoparticles in a hydroxyl-group functionalized ionic liquid: synthesis, characterization and catalytic performance. *Catal. Sci. Technol.* 5, 1683–1692. (doi:10.1039/c4cy01382d)
8. Ghosh S. 2004 Bimetallic Pt–Ni nanoparticles can catalyze reduction of aromatic nitro compounds by sodium borohydride in aqueous solution. *Appl. Catal. A* 268, 61–66. (doi:10.1016/j.apcata.2004.03.017)
9. Jiang HL, Akita T, Ishida T, Haruta M, Xu Q. 2011 Synergistic catalysis of Au@Ag core-shell nanoparticles stabilized on metal-organic framework. *J. Am. Chem. Soc.* 133, 1304–1306. (doi:10.1021/ja1099006)
10. O'Connor OA, Young LY. 1989 Toxicity and anaerobic biodegradability of substituted phenols under methanogenic conditions. *Environ. Toxicol. Chem.* 8, 853–862. (doi:10.1002/etc.5620081003)
11. Pradhan N, Pal A, Pal T. 2002 Silver nanoparticle catalyzed reduction of aromatic nitro compounds. *Colloids Surf. A* 196, 247–257. (doi:10.1016/s0927-7757(01)01040-8)
12. Rogers SM, Catlow CRA, Gianolio D, Wells PP, Dimitratos N. 2018 Supported metal nanoparticles with tailored catalytic properties through sol-immobilisation: applications for the hydrogenation of nitrophenols. *Faraday Discuss.* 208, 443–454. (doi:10.1039/c7fd00216e)
13. Aditya T, Pal A, Pal T. 2015 Nitroarene reduction: a trusted model reaction to test nanoparticle catalysts. *Chem. Commun. (Camb)* 51, 9410–9431. (doi:10.1039/c5cc01131k)
14. Wang C, Yang F, Yang W, Ren L, Zhang Y, Jia X, Zhang L, Li Y. 2015 PdO nanoparticles enhancing the catalytic activity of Pd/carbon nanotubes for 4-nitrophenol reduction. *RSC Adv.* 5, 27 526–27 532. (doi:10.1039/c4ra16792a)
15. Ma T, Liang F, Chen R, Liu S, Zhang H. 2017 Synthesis of Au–Pd bimetallic nanoflowers for catalytic reduction of 4-nitrophenol. *Nanomaterials (Basel)* 7, 239. (doi:10.3390/nano7090239)
16. Karki HP, Ojha DP, Joshi MK, Kim HJ. 2018 Effective reduction of p-nitrophenol by silver nanoparticle loaded on magnetic Fe₃O₄/ATO nano-composite. *Appl. Surf. Sci.* 435, 599–608. (doi:10.1016/j.apsusc.2017.11.166)
17. Ismail AA, Hakki A, Bahnemann DW. 2012 Mesostructure Au/TiO₂ nanocomposites for highly efficient catalytic reduction of p-nitrophenol. *J. Mol. Catal. A Chem.* 358, 145–151. (doi:10.1016/j.molcata.2012.03.009)
18. Aromal SA, Babu KV, Philip D. 2012 Characterization and catalytic activity of gold nanoparticles synthesized using ayurvedic arishtams. *Spectrochim. Acta A Mol. Biomol. Spectrosc.* 96, 1025–1030. (doi:10.1016/j.saa.2012.08.010)
19. Li B, Hao Y, Shao X, Tang H, Wang T, Zhu J, Yan S. 2015 Synthesis of hierarchically porous metal oxides and Au/TiO₂ nanohybrids for photodegradation of organic dye and catalytic reduction of 4-nitrophenol. *J. Catal.* 329, 368–378. (doi:10.1016/j.jcat.2015.05.015)
20. Schwank J. 1985 Gold in bimetallic catalysts. *Gold Bull.* 18, 2–10. (doi:10.1007/bf03214680)
21. Du Y, Cao N, Yang L, Luo W, Cheng G. 2013 One-step synthesis of magnetically recyclable rGO supported Cu@Co core-shell nanoparticles: highly efficient catalysts for hydrolytic dehydrogenation of ammonia borane and methylamine borane. *New J. Chem.* 37, 3035–3042. (doi:10.1039/c3nj00552f)
22. Wu T, Ma J, Wang X, Liu Y, Xu H, Gao J, Wang W, Liu Y, Yan J. 2013 Graphene oxide supported Au–Ag alloy nanoparticles with different shapes and their high catalytic activities. *Nanotechnology* 24, 125 301–125 311. (doi:10.1088/0957-4484/24/12/125301)
23. Zhang S, Shao Y, Liao H-G, Liu J, Aksay IA, Yin G, Lin Y. 2011 Graphene decorated with PtAu alloy nanoparticles: facile synthesis and promising application for formic acid oxidation. *Chem. Mater.* 23, 1079–1081. (doi:10.1021/cm101568z)
24. Yao W, Li F-L, Li H-X, Lang J-P. 2015 Fabrication of hollow Cu₂O@CuO-supported Au–Pd alloy nanoparticles with high catalytic activity through the galvanic replacement reaction. *J. Mater. Chem. A* 3, 4578–4585. (doi:10.1039/c4ta06378c)
25. Pozun ZD, Rodenbusch SE, Keller E, Tran K, Tang W, Stevenson KJ, Henkelman G. 2013 A Systematic investigation of p-nitrophenol reduction by bimetallic dendrimer encapsulated nanoparticles. *J. Phys. Chem. C Nanomater Interfaces* 117, 7598–7604. (doi:10.1021/jp312588u)
26. Cao E, Brett G, Miedziak PJ, Douthwaite JM, Barrass S, McMillan PF, Hutchings GJ, Gavrilidis A. 2017 A micropacked-bed multi-reactor system with in situ Raman analysis for catalyst evaluation. *Catal. Today* 283, 195–201. (doi:10.1016/j.cattod.2016.06.007)
27. Jiang H-L, Xu Q. 2011 Recent progress in synergistic catalysis over heterometallic nanoparticles. *J. Mater. Chem.* 21, 13 705–13 725. (doi:10.1039/c1jm12020d)

28. Lewis SA, Wilburn JP, Wellons MS, Cliffl DE, Lukehart CM. 2015 Carbon-supported AuPt and AuPd bimetallic nanocomposites as formic acid electrooxidation catalysts. *Phys. Status Solidi A* **212**, 2903–2909. (doi:10.1002/pssa.201532256)
29. Song HM, Anjum DH, Sougrat R, Hedhili MN, Khashab NM. 2012 Hollow Au@Pd and Au@Pt core-shell nanoparticles as electrocatalysts for ethanol oxidation reactions. *J. Mater. Chem.* **22**, 25 003–25 010. (doi:10.1039/c2jm35281h)
30. Carter JH, Althahban S, Nowicka E, Freakley SJ, Morgan DJ, Shah PM, Golunski S, Kiely CJ, Hutchings GJ. 2016 Synergy and anti-synergy between palladium and gold in nanoparticles dispersed on a reducible support. *ACS Catal.* **6**, 6623–6633. (doi:10.1021/acscatal.6b01275)
31. Fang W, Deng Y, Tang L, Zeng G, Zhou Y, Xie X, Wang J, Wang Y, Wang J. 2017 Synthesis of Pd/Au bimetallic nanoparticle-loaded ultrathin graphitic carbon nitride nanosheets for highly efficient catalytic reduction of p-nitrophenol. *J. Colloid Interface Sci.* **490**, 834–843. (doi:10.1016/j.jcis.2016.12.017)
32. Blosi M, Ortelli S, Costa AL, Dondi M, Lolli A, Andreoli S, Benito P, Albonetti S. 2016 Bimetallic nanoparticles as efficient catalysts: facile and green microwave synthesis. *Materials (Basel)* **9**, 550. (doi:10.3390/ma9070550)
33. Chen X, Cai Z, Chen X, Oyama M. 2014 AuPd bimetallic nanoparticles decorated on graphene nanosheets: their green synthesis, growth mechanism and high catalytic ability in 4-nitrophenol reduction. *J. Mater. Chem. A* **2**, 5668–5674. (doi:10.1039/c3ta15141g)
34. Srisombat L, Nonkumwong J, Suwannarat K, Kuntalue B, Ananta S. 2017 Simple preparation Au/Pd core/shell nanoparticles for 4-nitrophenol reduction. *Colloids Surf. A* **512**, 17–25. (doi:10.1016/j.colsurfa.2016.10.026)
35. Suwannarat K, Thongthai K, Ananta S, Srisombat L. 2018 Synthesis of hollow trimetallic Ag/Au/Pd nanoparticles for reduction of 4-nitrophenol. *Colloids Surf. A* **540**, 73–80. (doi:10.1016/j.colsurfa.2017.12.046)
36. Sun J, Fu Y, He G, Sun X, Wang X. 2014 Catalytic hydrogenation of nitrophenols and nitrotoluenes over a palladium/graphene nanocomposite. *Catal. Sci. Technol.* **4**, 1742–1748. (doi:10.1039/c4cy00048j)
37. Li WJ, Liang R, Hu AM, Huang ZH, Zhou YN. 2014 Generation of oxygen vacancies in visible light activated one-dimensional iodine TiO₂ photocatalysts. *Rsc Adv.* **4**, 36 959–36 966. (doi:10.1039/C4ra04768k)
38. Wang S, Zhang M, Zhang W. 2011 Yolk-shell catalyst of single Au nanoparticle encapsulated within hollow mesoporous silica microspheres. *ACS Catal.* **1**, 207–211. (doi:10.1021/cs1000762)
39. Cattaneo S, Freakley SJ, Morgan DJ, Sankar M, Dimitratos N, Hutchings GJ. 2018 Cinnamaldehyde hydrogenation using Au–Pd catalysts prepared by sol immobilisation. *Catal. Sci. Technol.* **8**, 1677–1685. (doi:10.1039/c7cy02556d)
40. Kou SF, Ye W, Guo X, Xu XF, Sun HY, Yang J. 2016 Gold nanorods coated by oxygen-deficient TiO₂ as an advanced photocatalyst for hydrogen evolution. *RSC Adv.* **6**, 39 144–39 149. (doi:10.1039/c6ra04444a)
41. Amaniampong PN, Li K, Jia X, Wang B, Borgna A, Yang Y. 2014 Titania-supported gold nanoparticles as efficient catalysts for the oxidation of cellobiose to organic acids in aqueous medium. *ChemCatChem* **6**, 2105–2114. (doi:10.1002/cctc.201402096)
42. Jia C, Yang P, Li J, Huang B, Matras-Postolek K. 2016 Photocatalytic activity evolution of different morphological TiO₂ shells on Ag nanowires. *ChemCatChem* **8**, 839–847. (doi:10.1002/cctc.201501045)
43. Dimitratos N *et al.* 2009 Oxidation of glycerol using gold-palladium alloy-supported nanocrystals. *Phys. Chem. Chem. Phys.* **11**, 4952–4961. (doi:10.1039/b904317a)
44. Pritchard J *et al.* 2010 Direct synthesis of hydrogen peroxide and benzyl alcohol oxidation using Au–Pd catalysts prepared by sol immobilization. *Langmuir* **26**, 16 568–16 577. (doi:10.1021/la101597q)
45. Konova P, Naydenov A, Venkov C, Mehandjiev D, Andreeva D, Tabakova T. 2004 Activity and deactivation of Au/TiO₂ catalyst in CO oxidation. *J. Mol. Catal. A Chem.* **213**, 235–240. (doi:10.1016/j.molcata.2003.12.021)
46. Chang F-W, Yu H-Y, Roselin LS, Yang H-C, Ou T-C. 2006 Hydrogen production by partial oxidation of methanol over gold catalysts supported on TiO₂-MO_x (M = Fe, Co, Zn) composite oxides. *Appl. Catal. A Gen.* **302**, 157–167. (doi:10.1016/j.apcata.2005.12.028)
47. Yang JH *et al.* 2005 Activation of Au/TiO₂ catalyst for CO oxidation. *J. Phys. Chem. B* **109**, 10 319–10 326. (doi:10.1021/jp050818c)

48. Radnik J, Mohr C, Claus P. 2003 On the origin of binding energy shifts of core levels of supported gold nanoparticles and dependence of pretreatment and material synthesis. *Phys. Chem. Chem. Phys.* **5**, 172–177. (doi:10.1039/b207290d)
49. Arrii S, Morfin F, Renouprez AJ, Rousset JL. 2004 Oxidation of CO on gold supported catalysts prepared by laser vaporization: direct evidence of support contribution. *J. Am. Chem. Soc.* **126**, 1199–1205. (doi:10.1021/ja036352y)
50. Villa A, Wang D, Veith GM, Vindigni F, Prati L. 2013 Sol immobilization technique: a delicate balance between activity, selectivity and stability of gold catalysts. *Catal. Sci. Technol.* **3**, 3036–3041. (doi:10.1039/c3cy00260h)
51. Desimoni E, Brunetti B. 2015 X-ray photoelectron spectroscopic characterization of chemically modified electrodes used as chemical sensors and biosensors: a review. *Chemosensors* **3**, 70–117. (doi:10.3390/chemosensors3020070)
52. Mei Y, Lu Y, Polzer F, Ballauff M, Drechsler M. 2007 Catalytic activity of palladium nanoparticles encapsulated in spherical polyelectrolyte brushes and core-shell microgels. *Chem. Mater.* **19**, 1062–1069. (doi:10.1021/cm062554s)
53. Hayakawa K, Yoshimura T, Esumi K. 2003 Preparation of gold-dendrimer nanocomposites by laser irradiation and their catalytic reduction of 4-nitrophenol. *Langmuir* **19**, 5517–5521. (doi:10.1021/la034339l)
54. Rajesh R, Venkatesan R. 2012 Encapsulation of silver nanoparticles into graphite grafted with hyperbranched poly(amidoamine) dendrimer and their catalytic activity towards reduction of nitro aromatics. *J. Mol. Catal. A Chem.* **359**, 88–96. (doi:10.1016/j.molcata.2012.04.001)
55. Motta D *et al.* 2019 Preformed Au colloidal nanoparticles immobilised on NiO as highly efficient heterogeneous catalysts for reduction of 4-nitrophenol to 4-aminophenol. *J. Environ. Chem. Eng.* **7**, 103381. (doi:10.1016/j.jece.2019.103381)
56. Gibson EK *et al.* 2015 Restructuring of AuPd nanoparticles studied by a combined XAFS/DRIFTS approach. *Chem. Mater.* **27**, 3714–3720.